I&EC research
Industrial & Engineering Chemistry Research

Article

pubs.acs.org/IECR

Binary Liquid−Liquid Equilibria for Systems of Mono- or Disubstituted Haloalkanes (Cl, Br) and Pyridinium-Based Ionic Liquids. Advances in the Experimentation and Interpretation of Results

Luís Fernández, Diego Montaño, Juan Ortega,* and Francisco J. Toledo

Laboratorio de Termodinámica y Fisicoquimica de Fluidos. Parque Científico-Tecnológico. Universidad de Las Palmas de Gran Canaria, Canary Islands, Spain

Supporting Information

ABSTRACT: This work presents the measurements made to define the temperature−composition curves for a set of binary systems composed of several pyridinium-based ionic liquids (ILs) [bpy][BF_4] and [b*Y*mpy][BF_4] (*Y* = 2,3,4) with mono- and dihaloalkanes (Cl and Br) in the temperature interval [280−473] K and at atmospheric pressure. With the exception of the short chain dichloroalkanes (1,1- and 1,2-), all the compounds present some degree of immiscibility with the ionic liquids selected. Solubility points (x_{IL},*T*) are determined by an image identification experimental procedure, which is described in detail and permits a more accurate definition of the liquid−liquid equilibria coexistence curves. A semiempirical model is proposed to correlate the experimental results of liquid−liquid equilibria (LLE) and the fits are compared with those obtained with the NRTL model. In both cases, a rigorous procedure is proposed to estimate LLE data considering the isoactivity criteria and a global test to guarantee the stability of the phases of the systems studied. H^1−NMR spectra are determined for some of the systems chosen to study the molecular interactions and their influence on the experimental results.

1. INTRODUCTION

Numerous theoretical and experimental studies have been conducted in recent years in an attempt to propose ionic liquids (ILs) as alternatives to current organic solvents. The low vapor pressures of ILs provide an added value to their possible uses, due to the fact that it facilitates their recovery and there is no risk of the emission of volatile pollutants. Nonetheless, to confirm their effectiveness it is important to conduct exhaustive experimentation designed to test their practical applications. One of the first experiments would consist in determining the intervals in which the ILs form homogeneous solutions with different types of solutes, as their behavior in solution can provide information about specific aspects of their structure. It is also important to establish the degree of miscibility between the substances involved, because this information affects the design of one of the most important separation operations in chemical engineering, liquid−liquid extraction,[1,2] in which the use of ILs has already been tested in laboratory. As mentioned previously, the knowledge begins with a miscibility study of the components to establish the zone of separation of one or two phases (LLE).

Previous works by our group have provided solubility data of systems composed of pyridinium-based ionic liquids with dibromoalkanes[3] and alkanols,[4−8] having presented measurements for the properties of miscible or partially miscible liquids. The studies of ILs with haloalkanes are especially useful to establish the interactional effects caused by these compounds. Since our experimentation requires more information relating to the dilution of dibromoalkanes,[3] this work aims to determine the miscibility of halides (mono- and di-) with a group of ILs with the pyridinium cation and the tetrafluoroborate anion, [bpy][BF_4] and [b*Y*mpy][BF_4] (*Y* = 2,3,4). The study was performed with monohalide $H_{2u+1}C_uX$ (*u* = 3−5) and dihalide $X(CH_2)_uX$ (*u* = 1−6) hydrocarbon solutions with X = Cl,Br, experimentally contributing to the definition of saturation curves for the LLE of these systems. The results are influenced not only by the nature of the IL used but also by the type of halogen (Cl,Br) and the number of these atoms present in the molecule. There are very few studies of the LLE curves of the selected systems published in the literature, except for the one cited previously[3] for dibromoalkanes. Nonetheless, several studies have published information about the LLE of pyridinium-based ILs with other organic compounds,[9−11] and of other ILs with other halide derivatives.[12−15]

The modeling was not easy in this study owing to the nonuniform distribution of the resulting curves. The NRTL model[16] is one of the most used to represent LLE data, and an extended version was used here.[17,18] The results are compared with those obtained with another polynomial model proposed here, which has produced excellent representations in other cases.[4]

2. EXPERIMENTAL SECTION

2.1. Materials. ILs [bpy][BF_4] and [b*Y*mpy][BF_4] (*Y* = 2,3,4) used were supplied by IOLITEC, GmbH & Co. KG, with a purity of 99+% w/w. To reduce the water contents of these products they were subjected to a slow distillation at vacuum.

Received: May 29, 2013
Revised: July 11, 2013
Accepted: July 11, 2013
Published: July 11, 2013

ACS Publications © 2013 American Chemical Society

dx.doi.org/10.1021/ie401710f | *Ind. Eng. Chem. Res.* 2013, 52, 11758−11766

Mono- and dihaloalkanes were supplied by Aldrich with purities close to 99+% w/w. All products were degasified with ultrasound and stored in the dark for several days on a Fluka molecular sieve of 0.3 nm to reduce the moisture. The final water content of all compounds was determined by a C-20 Karl Fisher titrator, and the final results are shown in Table S1 (Supporting Information) together with the values measured for other properties, such as the density ρ, and the refractive index n_D, at 298.15 K, which are compared with reference values. In general, the experimental values are in good agreement with published values.[4−33]

2.2. Apparatus and Procedures. The density of the pure compounds was measured using an Anton-Paar DMA-60/602 digital densimeter, with a reading error of ±0.005 kg·m^{-3}. The temperature was maintained stable at T = (298.15 ± 0.01) K with a 9012A Polyscience water thermostatic bath, which was also used to control the temperature of the apparatus during the measurements of n_D. A Zuzi 320 refractometer was used, with a reading error of ±0.0001.

Solubility data of the ILs+haloalkane systems were obtained by detecting the cloud point (change in turbidity) of the mixture. Reaching the equilibrium state (change of two phases to one phase or vice versa) depends on the mass transfer velocity between the two fluid phases, so homogenization was facilitated with a magnetic stirrer. Experimental determinations were made in the temperature range [280−473] K and at atmospheric pressure [98−99] kPa with the specific limitations to the characteristic of the components used. A scheme of the installation with a detailed explanation of its operation is given in the Appendix. Temperature measurements inside the LLE cell were made with an indication of ±1 mK, and an uncertainty less than ±0.03 K. Each point (x_{IL},T) is obtained by continuous dilution of the products of the binary mixture, checking that the compositions of each point presented uncertainties of (x ± 0.002).

For the binaries [bpy][BF_4]+1,ω-dichloroalkane (ω=1,2,3,4) ^{1}H NMR spectra were obtained at several compositions using a Bruker AMX 300 MHz apparatus. Chemical shifts δ of the signals were determined relative to the TMS reference signal (δ = 0). The samples were introduced in 5 mm NMR tubes and in a capillarythat the Cl_3CD required for the lock.

3. LLE RESULTS

In the presentation of experimental data, details are given for each group of mixtures together with some general observations about the results.

(ILs+1-Chloroalkane). The experimental values (x_{IL},T) of the systems [bpy][BF_4] and [bYmpy][BF_4] (Y = 2,3,4)+$C_nH_{2n+1}Cl$ (n = 3,4,5), are shown in Table S2 and represented in Figure 1 in the interval x_{IL} > 0.5. All the systems in this group present a partial miscibility. The miscibility increases with temperature and with the shortening of the monochloroalkane chain length; the corresponding curves present high slopes in the IL-rich regions. Measurements were not made to define the saturation curve in the monochloroalkane phase, since this curve almost coincides with the ordinate axis, showing that in this phase the solutions are not formed with x_{IL} above the uncertainty limit of the composition measurements, see section 2.2. In all cases, the UCST of the systems studied is much higher at the limiting temperature established for this study, of 473 K, exceeding the boiling point of chloroalkane. Another aspect observed is that the miscibility zone in the IL+1-chloroalkane solutions diminishes with the position of the methyl group −CH_3 in the pyridine ring, in the following order of isomers: Y=3,4 > Y = 2. The systems with [bpy][BF_4] are even more immiscible. The solutions of the same ILs with 1-chlorohexane produce completely immiscible solutions in the temperature range considered.

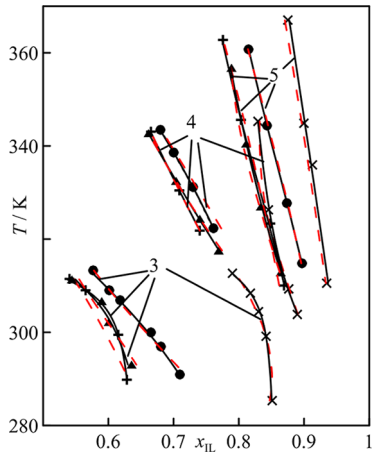

Figure 1. Experimental data and correlation curves for the binaries [bYmpy][BF4] + $CH_3(CH_2)_{n-1}Cl$ [Y = 0 (×), Y = 2 (●), Y = 3 (+), Y = 4 (▲)]. Labels indicate n. (—) proposed model (eq 3), (---) NRTL (eq 12).

(ILs+1-Bromoalkane). The coordinates corresponding to the solubility points were determined for the set of binary mixtures: [bpy][BF_4] or [bYmpy][BF_4] (Y = 2,3,4)+$C_nH_{2n+1}Br$ (n = 2−5). Measurements were not made for the bromomethane owing to its low boiling point (277 K) nor for the brominated derivatives with n > 5 owing to its high immiscibility. The experimental data (x_{IL},T) that produce the miscibility curve in the IL-rich zone, are shown in Supporting Information, Table S3 for each system; an identical observation to that made previously (see IL+1-chloroalkane) can be made for the binaries in the zone rich in bromoalkane; data are represented in Figure 2 panels a−d. The systems with [bpy][BF_4] present a greater immiscibility than those that contain methylated pyridinium derivates; of these, the ones in the meta and ortho positions are almost equal to the miscible ones with all the bromoalkanes, while the IL with the −CH_3 group in the para position dissolve more easily. In summary, the following order of immiscibility can be established for the group: [bpy][BF_4] > [b2mpy][BF_4] > [b3mpy][BF_4] > [b4mpy][BF_4]. A comparison of the curves in Figures 1 and 2 shows that, as expected, the monobromides are more immiscible than the corresponding monochlorides, which is related to the differences in size of the Cl and Br atoms and their electronegativities.

(ILs+α,ω-Dichloroalkane). Binary systems composed of ILs [bpy][BF_4] and [bYmpy][BF_4] with (Y = 2,3,4), and the first four dichloroalkanes 1,ω-Cl$(CH_2)_n$Cl with (ω = n = 2−4), are miscible over the entire range of compositions in the temperature interval [280−473] K, with the exception of the following systems: [bpy][BF_4]+1,3-dichloropropane, or +1,4-dichlorobutane, and [b2mpy][BF_4]+1,4-dichlorobutane, which are partially miscible. For these systems, the points that define the miscibility zone, obtained by direct experimentation (x_{IL},T), are shown in Supporting Information, Table S4 and are represented in Figure 3 panels a−d. All the systems generate binodal curves of the same typology and with values of UCST far above the range of working temperatures, except for those of

dx.doi.org/10.1021/ie401710f | Ind. Eng. Chem. Res. 2013, 52, 11758−11766

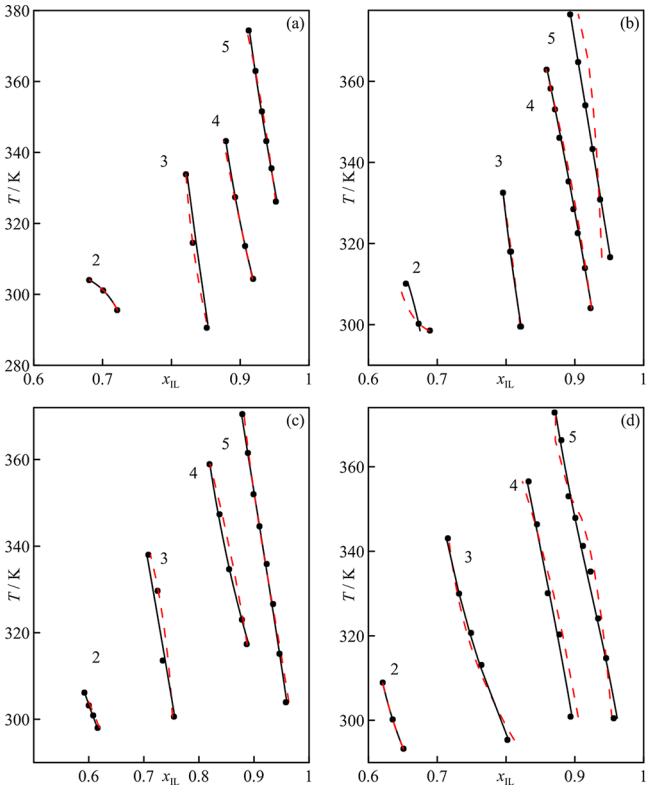

Figure 2. LLE Experimental data (•) obtained in this work and those from literature,[1] and the correlation curves corresponding to the binaries {[bpy][BF_4] or [bYmpy][BF_4] (Y = 2,3,4) + $H_{2n+1}C_nBr$}. Labels indicate *n*. (—) proposed model (eq 3), (---) NRTL (eq 12): (a) [bpy][BF_4]; (b) Y = 2; (c) Y = 3; (d) Y = 4.

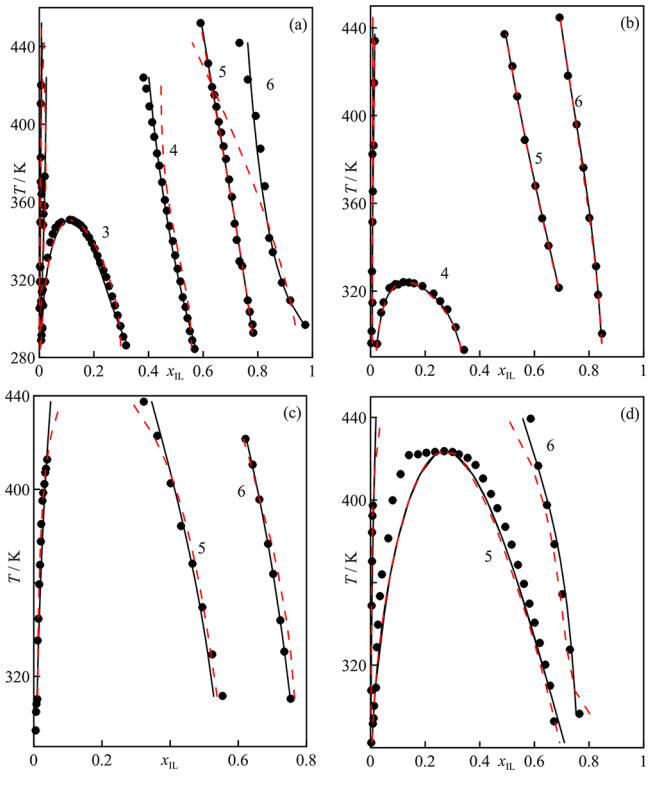

Figure 3. LLE Experimental data (•) obtained in this work and the correlation curves corresponding to the binaries {[bpy][BF_4] or [bYmpy][BF_4] (Y = 2,3,4) + Cl(CH_2)$_n$Cl}. Labels indicate *n*. (—) proposed model (eq 3), (---) NRTL (eq 12). (a) [bpy][BF_4]; (b) Y = 2; (c) Y = 3; (d) Y = 4.

the binaries [bpy][BF_4]+1,3-Cl(CH_2)$_3$Cl, (UCST: x_{IL} = 0.111, T = 350.79 K), [b2mpy][BF_4]+1,4-Cl(CH_2)$_4$Cl (UCST: x_{IL} = 0.120, T = 323.98 K), and [b4mpy][BF_4]+1,5-Cl(CH_2)$_5$Cl (UCST: x_{IL} = 0.269, T = 423.59 K). In all cases, the immiscibility increases with the chain length of the dichloroalkane, while for the same dichloroalkane, the systems with [bpy][BF_4] are more immiscible than the methylated ILs in the pyridine ring, establishing for the set the following order of immiscibility: [bpy][BF_4] > [b2mpy][BF_4] > [b3mpy][BF_4] ≈ [b4mpy][BF_4]. Comparing the results of Figures 1 and 3, the systems of pyridinium-based ILs with monochloroalkanes are generally more immiscible than the dichloroalkanes because the disubstituted compounds present a lower dipoles density than the monosubstituted compounds.

For this group the ^{1}H NMR spectra were determined for the mixtures [bpy][BF_4] + dichloromethane, + 1,2-dichloroethane, + 1,3-dichloropropane, and + 1,4-dichlorobutane and revealed slight diamagnetic or paramagnetic shifts for the protons as the concentration of the IL solution increased. These shifts that are represented as a function of the composition are mainly attributed to the anisotropy of the pyridine ring of the IL. Additional information is presented in the discussion section.

(IL+α,ω-Dibromoalkane). Supporting Information, Table S5 shows the solubility data for the systems [bpy][BF_4]+Br-(CH_2)$_n$Br (*n* = 1−5) and the corresponding representations in Figure 4a . The system [bpy][BF_4] + Br(CH_2)$_6$Br, is completely insoluble in the working range. The UCST of these systems increases regularly with the dibromide chain, except for 1,2-dibromoethane, which presents a binodal curve in an interval of compositions higher than that of 1,3-dibromopropane. The measurements corresponding to the group [bYmpy][BF_4](Y = 2−4) + Br(CH_2)$_n$Br (*n* = 2−6) are shown in Figure 4 panels b−d and correspond to two sets of experimental determinations: those obtained in this work for zones rich in dibromoalkane and those obtained from a previous study[3] determined in zones rich in IL. The quantities of both data sets appear in Supporting Information, Table S5. The systems [bYmpy][BF_4] (Y = 2,3,4) + dibromomethane are completely soluble in the working range selected. The degree of immiscibility for the set of ILs, when the same dibromoalkane is analyzed, can be arranged in the following order: [bpy][BF_4] > [b2mpy][BF_4] > [b3mpy][BF_4] > [b4mpy][BF_4] in the first alkyl dibromides, but this becomes slightly inverted to [bpy][BF_4] > [b2mpy][BF_4] > [b4mpy][BF_4] > [b3mpy]-[BF_4] after 1,5-dibromopentane. The dibromoalkanes are more insoluble than the dichloroalkanes for the same reasons given previously for the monosubstituted ones.

In general, studies carried out with bromide compounds present certain limitations in relation to working temperatures, since the solution takes on a dark red color caused by the bromine liberation (verified by decoloration with 10% sodium bisulphite).

4. CORRELATION OF LLE EXPERIMENTAL DATA

4.1. Presentation of Models. The correlation of LLE experimental data (x_{IL},T) was not carried out directly but in relation to excess Gibbs function g^E. Values for the activity coefficients γ_i of the LLEs cannot be obtained from the information available in Supporting Information, Tables S2−S5, so the fit cannot be done directly. The isoactivity criterion is

dx.doi.org/10.1021/ie401710f | Ind. Eng. Chem. Res. 2013, 52, 11758−11766

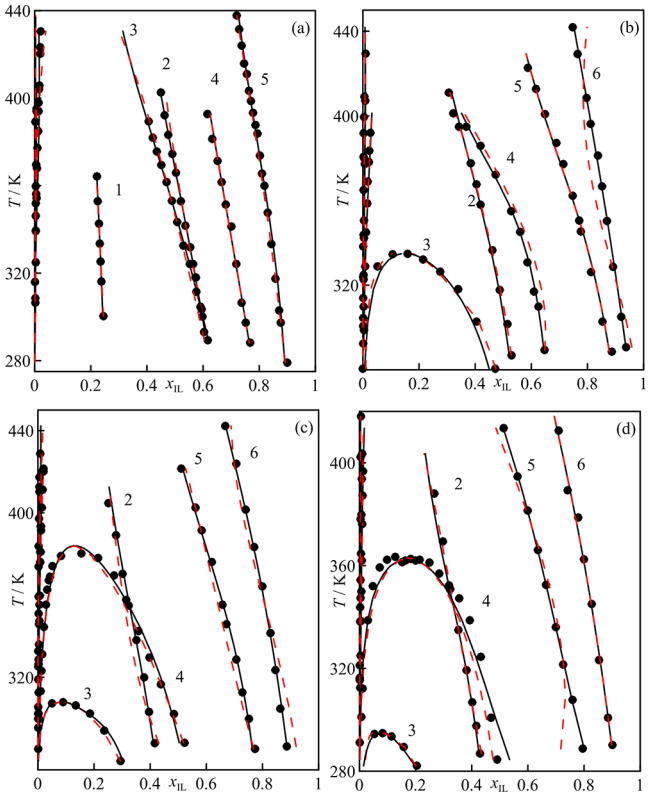

Figure 4. LLE experimental data (•) obtained in this work and those from literature,[3] and the correlation curves corresponding to the binaries {[bpy][BF_4] or [bYmpy][BF_4] (Y = 2,3,4) + Br(CH_2)$_n$Br}. Labels indicate *n*. (—) proposed model (eq 3), (---) NRTL (eq 12). (a) [bpy][BF_4]; (b) Y = 2; (c) Y = 3; (d) Y = 4.

established as a prerequisite to verify liquid−liquid equilibria and is expressed in terms of γ_i for two liquid phases (I and II). For the case of a binary mixture, this criterion, at known *p* and *T* given, is represented by

$$\left.\begin{aligned} x_1^{\mathrm{I}}\gamma_1^{\mathrm{I}}(x_i^{\mathrm{I}}, T, p) &= x_1^{\mathrm{II}}\gamma_1^{\mathrm{II}}(x_i^{\mathrm{II}}, T, p) \\ x_2^{\mathrm{I}}\gamma_2^{\mathrm{I}}(x_i^{\mathrm{I}}, T, p) &= x_2^{\mathrm{II}}\gamma_2^{\mathrm{II}}(x_i^{\mathrm{II}}, T, p) \end{aligned}\right\} \quad (1)$$

where x_i^{I} and x_i^{II} are the conjugated molar fractions of component *i* in the two liquid phases in equilibrium; an analogous significance to the activity coefficients γ_i^{I} and γ_i^{II}. Hence, a mathematical equation must be considered that incorporates the different compositions, the most appropriate being the dimensionless excess Gibbs function,

$$\frac{g^{\mathrm{E}}}{RT} = \sum_{i=1}^{2} x_i \ln \gamma_i \quad (2)$$

Now, a mathematical model must be used for g^{E} together with the system of eqs 1. In practice the procedure is quite complex since different solutions can be found for eq 1 that are mathematically valid but do not strictly comply with the thermodynamic criterion. For this reason, a procedure described in a previous work[4] was employed, which proposes to use a polynomial model to represent g^{E} (*x*,*T*) in terms that contain an active fraction "*z*", which is dependent on the composition. The generic form of the model relating to compound 1 of a binary is

$$\frac{g^{\mathrm{E}}}{RT} = z_1(1 - z_1)\sum_{i=0}^{r} g_i(T) z_1^i = z_1(1 - z_1)\sum_{i=0}^{r} g_i(T)\left[\frac{x_1}{(x_1 + kx_2)}\right]^i \quad (3)$$

where *k* is a parameter characteristic of the mixture that can be considered to be independent of temperature,[34,35] so in the correlation process it is considered as an additional coefficient to the $g_i(T)$. Depending on the difficulty to fit the data, a simple relationship may be established for the coefficients $g_i(T)$. In this case, the following expression was sufficient:

$$g_i(T) = \frac{g_{i1}}{T} + g_{i2} \quad (4)$$

From eq 3 a generic expression can be obtained for the activity coefficients. Considering that

$$RT \ln \gamma_i = \bar{g}_i^{\mathrm{E}} = g^{\mathrm{E}} - \sum_{k\neq i}^{N} x_k \left(\frac{\partial g^{\mathrm{E}}}{\partial x_k}\right)_{p,T,x_{j\neq k,i}} \quad (5)$$

Equation 3 gives rise to a specific equation for the γ_j.

$$\ln \gamma_j = z_1(1 - z_1)\sum_{i=0}^{r} g_i(T) z_1^i + (2 - j - x_1)k\left(\frac{z_1}{x_1}\right)^2 Y(x_1, T) \quad (6)$$

where

$$Y(x_1, T) = (1 - 2z_1)\sum_{i=0}^{r} g_i(T) z_1^i + z_1(1 - z_1)\sum_{i=1}^{r} i g_i(T) z_1^{i-1} \quad (7)$$

To obtain the coefficients of fit g_{ij}, for eq 4, a two-step procedure was proposed:

I. Isoactivity criterion. In this step, optimum values are obtained for the g_{ij} parameters of the model that fulfills the isoactivity criterion established with eqs 1. A genetic algorithm (GA) is used optimizing the following objective function $(\mathrm{OF})_\gamma$,

$$(\mathrm{OF})_\gamma = \sum_{j=1}^{m}\sum_{i=1}^{2}\left[x_{ij}^{\mathrm{I}}\gamma_{ij}^{\mathrm{I}}(x_{ij}^{\mathrm{I}}, T_j, p) - x_{ij}^{\mathrm{II}}\gamma_{ij}^{\mathrm{II}}(x_{ij}^{\mathrm{II}}, T_j, p)\right]^2 \quad (8)$$

where *m* is the number of experimental data. Using this objective function it is possible to verify the quality of the conjugated compositions that were estimated by interpolation of experimental data. These values are used as starting values in the next step.

II. Phase stability criterion. With the compositions estimated in the previous step, an interative calculation was performed to determine the real conjugated compositions. The GA is used to minimize the following objective function:

$$(\mathrm{OF})_x = \sum_{j=1}^{m}\sum_{i=2}^{2}\left[(x_{ij,\mathrm{exp}}^{\mathrm{I}} - x_{ij,\mathrm{cal}}^{\mathrm{I}}) - (x_{ij,\mathrm{exp}}^{\mathrm{II}} - x_{ij,\mathrm{cal}}^{\mathrm{II}})\right] \quad (9)$$

dx.doi.org/10.1021/ie401710f | Ind. Eng. Chem. Res. 2013, 52, 11758−11766

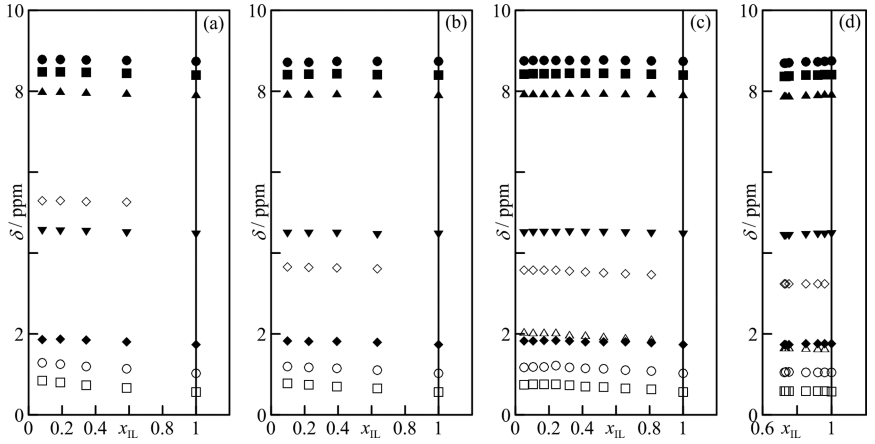

Figure 5. Representation of the chemical shifts, δ, as a function of IL composition in the solutions of [bpy][BF_4] + (a) $Cl(CH_2)Cl$, (b) $Cl(CH_2)_2Cl$, (c) $Cl(CH_2)_3Cl$, (d) $Cl(CH_2)_4Cl$: (●) H_a, (■) H_b, (▲) H_c, (▼) H_d, (♦) H_e, (○) H_f, (□) H_g, (◊) H_h, (△) H_i.

that is established to determine the differences between the conjugated compositions in both phases, obtained in the experimentation, and the values calculated using the parametric model for the activity coefficients, eq 6. The $x^{I}_{ij,cal}$ are obtained by solving the system of eqs 1 by the Newton−Raphson method. Even then, not all the solutions obtained with this procedure are valid, since the isoactivity between phases does not guarantee the stability. For compliance in this second step an even more rigorous condition, in thermodynamic terms, is added to the minimization process, based on the stability criterion between phases. This criterion, established for the excess Gibbs function is

$$\left(\frac{\partial^2 g^E}{\partial x_1^2}\right)_{p,T} + \frac{RT}{x_1 x_2} > 0 \tag{10}$$

or through the activity coefficients,

$$\frac{1}{x_i} + \left(\frac{\partial \ln \gamma_i}{\partial x_i}\right)_{p,T} > 0 \tag{11}$$

The minimization method is applied with a GA that guarantees a convergence for the parameters of the model. To study the goodness of the application using the proposed model, the results were compared with those obtained from the NRTL model,[16] frequently used in the treatment of LLE data,

$$\frac{g^E}{RT} = x_1 x_2 \left(\frac{\tau_{21} G_{21}}{x_1 + G_{21} x_2} + \frac{\tau_{12} G_{12}}{G_{12} x_1 + x_2}\right) \tag{12}$$

which gives rise, according to eq 5, to a generic expression for the γ_i.

$$\ln \gamma_i(x_i, T) = x_j^2 \left[\tau_{ji}\left(\frac{G_{ji}}{x_i + G_{ji} x_j}\right)^2 + \frac{\tau_{ij} G_{ij}}{(G_{ij} x_i + x_j)^2}\right] \tag{13}$$

The G_{ij} parameters are related with the τ_{ij} by a simple exponential, $G_{ij} = \exp(-\alpha\tau_{ij})$ where α is the nonrandomness parameter. In the original model[16] an expression of the type $\tau_{ij} = \Delta g_{ij}/RT$ is used, although this is not adequate to perform the data correlation in this work, and an extended form[17,18] is required to obtain the best fits

$$\ln G_{ij} = -\alpha\left(\Delta g_{ij1} + \frac{\Delta g_{ij2}}{T} + \Delta g_{ij3} \ln T\right) \tag{14}$$

The model now presents seven adjustable parameters, six with energetic significance Δg_{ijk}, which model the variation in the molecular interactions with the temperature of the system, and α. The mathematical procedure to fit the experimental data to the NRTL equation is the same as the one described previously for the model proposed here.

4.2. Mathematical Treatment of Experimental LLE Data. All the experimental LLE data for the binary systems formed by [bpy][BF_4] and [bYmpy][BF_4] (Y = 2,3,4) with mono- and dihalide hydrocarbons of chlorine and bromine, compiled in Supporting Information, Tables S2−S5, were correlated using the procedure described in detail in the previous section, with eqs 3 and 12. The results obtained are recorded in Supporting Information, Table S6, which shows the parameters of the models and the standard deviations of each binary system, calculated in relation to the composition of the IL by the following expression:

$$s(x_{IL}) = \left[\left(\sum_{j=1}^{m} \left[(x^{I}_{ILj,exp} - x^{I}_{ILj,cal})^2 + (x^{II}_{ILj,exp} - x^{II}_{ILj,cal})^2\right]\right) / 2m\right]^{1/2} \tag{15}$$

where m is the number of experimental points in either phase I or II. Figures 1−4 show the representations obtained with the two models used. In general, the proposed model, eq 3, gives good correlations for the LLE data of the different mixtures, with the exception of the binary system [b4mpy][BF_4] + 1,5-$Cl(CH_2)_5Cl$, which presents a horizontal plateau that makes it difficult to define the UCST, with a deviation of $s(x_{IL}) > 0.03$; the deviation calculated for the NRTL model is greater. This model produces large deviations in most of the systems studied. In some cases, such as for [b2mpy][BF_4] + $CH_3(CH_2)_3Br$ and [b4mpy][BF_4] + $CH_3(CH_2)_4Br$, quantitatively valid fits are achieved but the curve "oscillates" between the data, giving nonrealistic representations, see Figure 2. The representation with NRTL of the system [bpy][BF_4]+$Cl(CH_2)_6Cl$ is not adequate either, Figure 3a, with $s(x_{IL}) > 0.07$.

dx.doi.org/10.1021/ie401710f | Ind. Eng. Chem. Res. 2013, 52, 11758−11766

5. DISCUSSION

From the experimental data obtained here together with data published in the literature on IL systems with haloalkanes,[12−15] some conclusions can be drawn about their behavior and the resulting LLE curves produced. Qualitatively, the systems studied present very similar characteristics for the binodal curves, exhibiting a variation in temperature that follows an order that depends on the chain of the halide compound, with the occasional exception. So, the UCST cannot be defined for most of the systems as it exceeds the range of temperatures used in the experimentation. The binary systems $\{x_1[bYmpy][BF_4]$ $(Y = 0,2,3,4) + x_2C_nH_{2n+1}X$ or $+x_2X(CH_2)_nX$ (X = Cl, Br; $n = 2−6)\}$ show small changes in solubility with T, in other words, with the higher values of the slope (dT/dx_1). In general, monosubstituted compounds are less soluble in the ILs than disubstituted compounds, which is especially critical in the haloalkane-rich phase, where the limits of the composition are below the limit of experimental uncertainty. An increase in chain length of the monohaloalkane $C_nH_{2n+1}X$ diminishes its solubility in the ILs owing to the increased contact surface between the molecules of the monosubstituted compound, which is stabilized by the van der Waals attractions and by the decrease of dipole density. This reduction caused by the dihaloalkane has been correlated with the decreased chemical shifts of the hydrogens H_h (δ 5.26 → δ 3.61 → δ 3.48 → δ 3.24) and H_i (δ 1,90 → δ 1,66) in the ^{1}H NMR spectra (Figure 5) of the mixtures of $C_nH_{2n}Cl_2$+[bpy][BF_4] at 80% v/v in the IL, for n = 1, 2, 3, 4, respectively. The changes in the chemical shifts in ^{1}H NMR spectra are related to dipoles density and therefore solubility. Nonetheless, for the $Cl(CH_2)_nCl$ + [bpy][BF_4] (n = 1−3) systems, shifts are presented at other compositions, Figure 5(a−c), while for the system $Cl(CH_2)_4Cl$ + [bpy][BF_4] shifts are shown in Figure 5d, from $x_{IL} > 0.6$.

Moreover, an increase in n in $C_nH_{2n+1}X$ implies that this compound will have more difficulty introducing itself among the molecules of the IL (see Figure 6), occupying more space and providing a greater impediment and an increased immiscibility, although this aspect should also be considered in relation to the dihaloalkane chain $C_nH_{2n}X_2$. In the opposite case, as the n of the mono- or disubstituted hydrocarbon decreases, this can introduce among the molecules of the IL more easily, an increase in the intermolecular distance d, and the generation of a drop in the ion−ion interactions, which is translated into endothermic mixing processes, as published previously.[3] However, exceptions to this behavior can be observed with the 1,2-dibromoethane that presents a lower solubility than the 1,3-dibromopropane, and even than the 1,4-dibromobutane; in the latter case, at temperatures higher than 346, 355, and 409 K, which correspond to cut off points with the systems of [b4mpy][BF_4], [b3mpy][BF_4] and [b2mpy]-[BF_4], respectively. This effect is attributed to a canceling out of the two dipoles associated with the C−Br bonds of the *anti*-conformation of the dibromoethane, giving rise to a decrease in the ion−dipole interactions in the final product.

By setting the degree of halogenation and the same chain length (identical density of C−X dipoles), the halides with the most electronegative heteroatoms are the most soluble; hence, the $C_nH_{2n}Cl_2$ are more soluble than the $C_nH_{2n}Br_2$. These observations in the experimental results were as expected given the magnitude of the corresponding dipoles $C^{\delta+}−X^{\delta-}$ (μ = 1.896 D for the $CH_3{}^{35}Cl$ and μ = 1.822 D for the $CH_3{}^{79}Br$) (see ref 36). In regard to the IL, incorporation of a methyl group in the structure of the pyridine ring increases its liposolubility, and the magnitude of this effect depends on the position of this group, with the following order being established: para substituted (Y = 4) > meta substituted (Y = 3) > ortho substituted (Y = 2). In summary the methylated substitution in ILs relates to the dilution in terms of van der Waals forces. Several authors[37,38] propose that the ILs form organized nanostructures, where the presence of the methyl group improve the solubility.

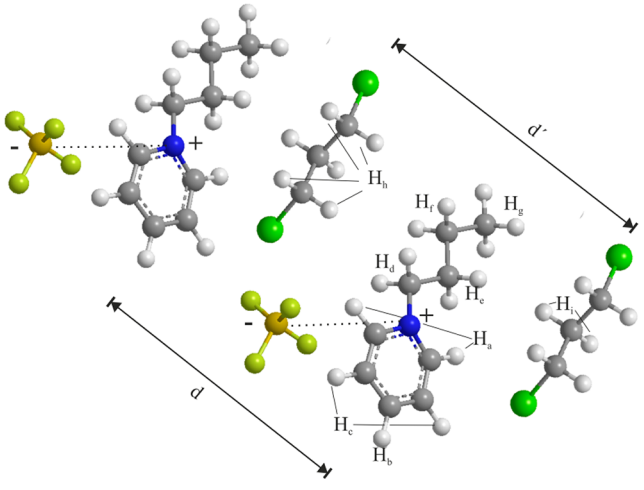

Figure 6. Representation of the structural model indicating the interactions between [bpy][BF_4] and $Cl(CH_2)_3Cl$. In the scheme are identified each of the proton groups considered in ^{1}H NMR.

APPENDIX

A.1. Experimental Apparatus

The methodology designed for this work requires an experimental installation composed of several elements. The visual detection procedure used previously[4,8] has been improved for this study by employing a digitalized optical system to avoid human errors. Figure A1 shows a scheme of how the different pieces of equipment are connected to each other. The equilibrium cell (1) is concentric with another of larger diameter and between the two cells a thermal fluid from a 1190 Polyscience thermostatic water bath circulates. The temperature is measured directly with a Pt-100 thermoresistance connected to an ASL-F25 digital thermometer, with (T

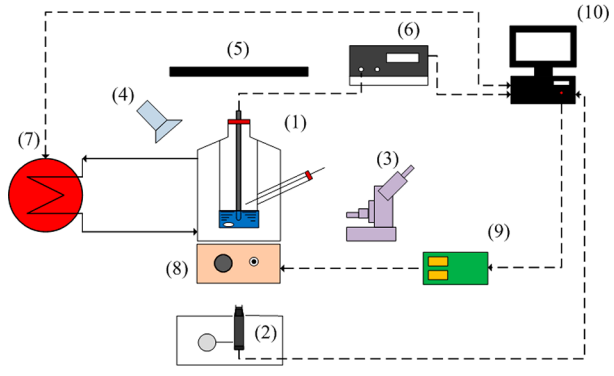

Figure A1. Diagram of the installation: (1) liquid−liquid equilibrium cell, (2) digital microscope, (3) magnifying glass, (4) light source, (5) plane-background, (6) digital thermometer, (7) water bath, (8) magnetic stirrer, (9) communication interface CEBEK T-5, (10) PC.

dx.doi.org/10.1021/ie401710f | *Ind. Eng. Chem. Res.* 2013, 52, 11758−11766

±0.01) K. Turbidity changes are detected by two procedures: (a) a focused powerful magnifying lens, and (b) the use of a 5 Mpixel digital camera. The entire operation is controlled by software specially designed for this work, implemented in MATLAB. The composition of the sample in the cell is known, and a detailed description of the procedure followed is given below.

A.2. Experimental Procedure

The solubility points (x_A,T), at a specific pressure of two generic compounds A+B are obtained by following a continuous addition methodology starting with a known quantity of one of these, such as A, in the main cell. Previously measured quantities of substance B are added using a Hamilton TLL 100 μL precision syringes, or also calculated by differences of weight. The dissolution of A + B is facilitated by a magnetic stirrer and by heating or cooling until the two phases homogenize to form a single phase, validating the point (x_A,T) measured. B is added again, and the operation is repeated until compositions of the mixture close to $x_A = 0.5$ are reached. Then, the reverse process is then carried out, in other words, by first introducing a known quantity of substance B in the cell and adding small known amounts of A, calculating the compositions in the interval of $x_A < 0.5$. The interval of compositions is completed in this way to define the miscibility curve. It was verified on numerous occasions that the compositions calculated at each point presented uncertainties less than 0.002.

Since the exact detection of the point of change must be independent of the visual quality of the investigator an *ad-doc* procedure controlled by PC was prepared, which functions as follows. When one liquid is added to another, as described above, the software designed to identify the different images appearing is activated. The magnifying glass, see Figure A1, estimates an approximate transition temperature; and therefore an image identification procedure to accurately observe the objective point is used. The identification process has two steps, one corresponding to the thermal programming and another to automatic image identification.

In the first step, a program is set up to study over a given temperature interval, $\Delta T = T_2 - T_1$, the photographic behavior of the solution in the LLE cell is then analyzed. After reaching a minimum temperature T_1, which can be previously estimated by the magnifying glass, the temperature is gradually raised by the water bath as the PC records an image at each 0.05 K, in other words, it records 20 images/degree, generating a photographic history. This scanning can be improved even further by using a digital camera with a higher resolution and a PC with a high storage capacity, which could be employed in future research. An exhaustive analysis of these photographic records enables us to identify the solubility temperature. Selection of this temperature is done in two ways: visually, from the records obtained, since the visual observation is improved by using a magnifying glass, or by using an algorithm that analyzes the sequence of images and determines, from a characteristic value, the solubility point automatically.

Identification Algorithm. An equilibrium point has been detected by analyzing the photographic records of an experiment. Now it is important use a tool designed to extract information from the solubility state; hence, before starting any program, the system must be "shown" how to acquire the symptoms of insolubility to achieve an optimum resolution of the objective point. The photographs taken by the digital camera used in this work are in color, in other words, they are in RGB format, but have been mathematically treated with a gray scale. An image on the gray scale is digitalized as a matrix, where each element quantifies the light intensity of one pixel, expressed as a number between 0 (opaque black) and 255 (brilliant white). Figure A2 shows an image on the gray scale and its associated matrix.

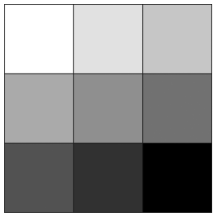

$$\begin{bmatrix} 255 & 220 & 190 \\ 160 & 130 & 100 \\ 70 & 30 & 0 \end{bmatrix}$$

Figure A2. Description of an image on the gray scale.

Digitalization translates the image into a set of numbers, which can be identified on the predetermined scale. There are various mathematical methods to extract this digitalization, which also permit editing of the images (color corrections, design effects, etc). It is important to associate the effects of the insolubility (referred to previously) to values of the matrices that can be obtained from the successive images; if the liquid is opaque the intensity of light is very different to when it is translucent. This phenomen stands out more when a background is chosen that contrasts with the cloud. Therefore, the state of the sample can be identified from a measurement of the light intensity in the cell. The next step consists in measuring the mean light intensity of all the pixels $\overline{I}$, and the standard deviation of each pixel $s(I)$, in relation to that mean value. The process is repeated for each of the images, and related to the temperature at which it was measured; in this way a series of tabulated data are obtained $[T,\overline{I}, s(I)]$ that are used to produce the representations made in this work.

To validate the method developed, the results obtained in this work were compared with those of methanol + hexane recorded in the literature.[39,40] The digital identification graph of the LLE for the methanol + hexane system can be seen in Figure A3 (for a solution of composition $x = 0.684$ in methanol) which illustrates the distribution of experimental points corresponding to the light intensity I, versus temper-

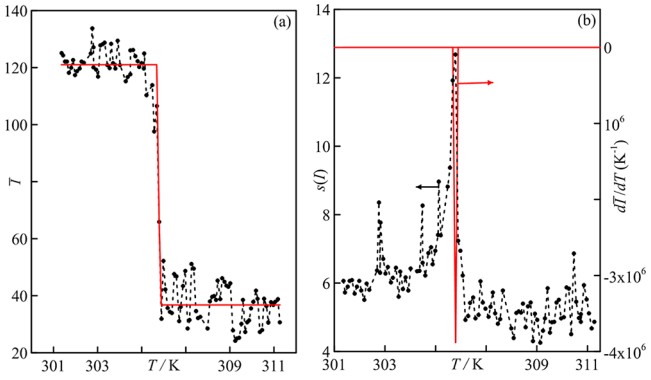

Figure A3. Values obtained to determine the solubility of the methanol(1) + hexane(2) mixture at a composition of $x_1 = 0.684$. (a) Mean light intensity (●) and correlation by eq A1. The insolubility-solubility situations are illustrated by two photographs. (b) Shift in light intensity (●), $s(I)$, and derivative of the mean intensity in relation to T (—).

dx.doi.org/10.1021/ie401710f | *Ind. Eng. Chem. Res.* 2013, 52, 11758−11766

ature, showing a sharp drop at the value I, when passing from a situation of clear insolubility at low temperatures (<33 °C) (intense white mist), to another soluble one, at approximately 34.5 °C (black background). The shift also presents a characteristic behavior showing a pronounced peak caused by partial disappearance of the mist, Figure A3b.

The step simulation produced, Figure A3a, can be carried out using an expression that is often employed in electronics to mathematically represent step-current impulses. This equation has the following form:

$$\bar{I} = \frac{C_0}{C_1 + \exp(C_2 T + C_3)} + C_4 \quad \text{(A1)}$$

Where T/K is the temperature and C_i are the coefficients to be determined in a nonlinear regression procedure. After obtaining the values of C_i, the model (A1) reproduces the step (in red) of the figure, clearly showing the jump between the two situations or states (one or two phases). It is interesting to determine the precise temperature at which the change between both states occurs. A simple method consists in analyzing the slope of light intensity, in other words the one derived from expression (A1), which produces a minimum at a given value of T, that represents the temperature of the change, see Figure A2b. The value obtained in this case is T = 305.79 K, which is quite close to values estimated in experiments carried out by other authors (305.71 K,[39] 305.62 K[40]).

■ ASSOCIATED CONTENT

Supporting Information

Table (S1) contains the experimental values of pure compounds and Tables (S2) to (S5) contain the solubilities for the binary systems studied. This material is available free of charge via the Internet at http://pubs.acs.org.

■ AUTHOR INFORMATION

Corresponding Author

*E-mail: jortega@dip.ulpgc.es.

Notes

The authors declare no competing financial interest.

■ ACKNOWLEDGMENTS

This work was carried out with financial support from the Spanish MICINN (project CTQ2009-12482).

■ NOMENCLATURE

GA = genetic algorithm
G_{ij} = parameters of NRTL equation
g^E = excess molar Gibbs energy function, J·mol^{-1}
g_i = coefficients of eqs 3,4
g_{ij} = coefficients of eqs 4
I, II = liquid phases
IL = ionic liquid
k = parameter of eq 3
OF = objective function
p = pressure, kPa
R = gas constant, kJ·kmol^{-1}K^{-1}
$s(x)$ = standard error of mole fraction, eq 15
T = Temperature, K
UCST = upper critical solution temperature, K
x = set of experimental data of LLE
x_{IL} = ionic liquid mole fraction
n = haloalkane chain length
Y = factor of eq 6 defined by eq 7
z_i = active fraction of component i in eq 3

Cations

[bpy]$^+$ = [butylpyridinium]$^+$
[b2mpy]$^+$ = [butyl-2-methylpyridinium]$^+$
[b3mpy]$^+$ = [butyl-3-methylpyridinium]$^+$
[b4mpy]$^+$ = [butyl-4-methylpyridinium]$^+$

Anions

[BF_4]$^-$ = [tetrafluoroborate]$^-$

Greek Letters

α = nonrandom parameter of NRTL equation
Δg_{ij1}, Δg_{ij2} and Δg_{ij3} = coefficients of eqs 16 and 17
γ_i = activity coefficient of component i
τ_{ij} = coefficients of NRTL equation

■ REFERENCES

(1) Domínguez, I.; González, E. J.; González, R.; Domínguez, A. Extraction of Benzene from Aliphatic Compounds Using Commercial Ionic Liquids as Solvents: Study of the Liquid−Liquid Equilibrium at T = 298.15 K. *J. Chem. Eng. Data* **2011**, *56*, 3376−3383.

(2) Revelli, A. L.; Mutelet, F.; Jaubert, J.-N. Extraction of *n*-Alcohols from *n*-Heptane Using Ionic Liquids. *J. Chem. Eng. Data* **2011**, *56*, 3873−3880.

(3) Navas, A.; Ortega, J.; Palomar, J.; Diaz, C.; Vreekamp, R. COSMO-RS analysis on mixing properties obtained for the systems 1-butyl-*X*-methylpyridinium tetrafluoroborate [X = 2,3,4] and 1,ω-dibromoalkanes [ω = 1−6]. *Phys. Chem. Chem. Phys.* **2011**, *13*, 7751−7759.

(4) Espiau, F.; Ortega, J.; Fernández, L.; Wisniak, J. Liquid−liquid equilibria in binary solutions formed by [pyridinium-derived][F4B] ionic liquids and alkanols: New experimental data and validation of a multiparametric model for correlating LLE data. *Ind. Eng. Chem. Res.* **2011**, *50*, 12259−12270.

(5) Ortega, J.; Vreekamp, R.; Marrero, E.; Penco, E. Thermodynamic properties of 1-butyl-3-methylpyridinium tetrafluoroborate and its mixtures with water and alkanols. *J. Chem. Eng. Data* **2007**, *52*, 2269−2276.

(6) Ortega, J.; Vreekamp, R.; Penco, E.; Marrero, E. Mixing thermodynamic properties of 1-butyl-4-methylpyridinium tetrafluoroborate [b4mpy][BF4] with water and with an alkan-1-ol (methanol to pentanol). *J. Chem. Thermodyn.* **2008**, *40*, 1087−1094.

(7) Navas, A.; Ortega, J.; Vreekamp, R.; Marrero, E.; Palomar, J. Experimental thermodynamic properties of 1-butyl-2-methylpyridinium tetrafluoroborate [b2mpy][BF4] with water and with alkan-1-ol and their interpretation with the COSMO-RS methodology. *Ind. Eng. Chem. Res.* **2009**, *48*, 2678−2690.

(8) Vreekamp, R.; Castellano, D.; Palomar, J.; Ortega, J.; Espiau, F.; Fernandez, L.; Penco, E. Thermodynamic behavior of the binaries 1-butylpyridinium tetrafluoroborate with water and alkanols: Their interpretation using ^{1}H-NMR spectroscopy and quantum-chemistry calculations. *J. Phys. Chem. B* **2011**, *115*, 8763−8774.

(9) Letcher, T. M.; Ramjugernath, D.; Tumba, K.; Królikowski, M.; Domanska, U. (Solid+liquid) and (liquid+liquid) phase equilibria study and correlation of the binary systems {*N*-butyl-3-methylpyridinium tosylate+water, or +an alcohol, or +a hydrocarbon}. *Fluid Phase Equilib.* **2010**, *294*, 89−97.

(10) Meindersma, W.; van Acker, T.; de Haan, A. B. Physical properties of 3-methyl-*N*-butylpyridinium tricyanomethanide and ternary LLE data with an aromatic and an aliphatic hydrocarbon at T = (303.2 and 328.2) K and p = 0.1 MPa. *Fluid Phase Equilib.* **2011**, *307*, 30−38.

(11) Jongmans, M. T. G.; Raijmakers, M.; Schuur, B.; de Haan., A. B. Binary and ternary vapor−liquid equilibrium data of the system (ethylbenzene + styrene + 4-methyl-*N*-butylpyridinium tetrafluoroborate) at vacuum conditions and liquid−liquid equilibrium data of their binary systems. *J. Chem. Eng. Data* **2012**, *57*, 626−633.

(12) Shiflett, M. B.; Yokozeki, A. Solubility differences of halocarbon isomers in ionic liquid [emim][Tf2N]. *J. Chem. Eng. Data* **2007**, *52*, 2007−2015.
(13) Deive, F. J.; Rodríguez, A.; Pereiro, A. B.; Shimizu, K.; Forte, P. A. S.; Romaño, C. C.; Canonjía Lopes, José N.; Esperança, J. N.; Rebelo, J. M. S. S.; Phase, L. P. N. Equilibria of haloalkanes dissolved in ethylsulfate- or ethylsulfonate-based ionic liquids. *J. Phys. Chem. B* **2010**, *114*, 7329−337.
(14) Cai, S.; Wang, L.; Yang, G.; Li, Y. Solubilities of 1-methyl-3-(3-sulfopropyl)-imidazolium hydrogen sulfate in selected solvents. *Chin. J. Chem. Eng.* **2010**, *18*, 1008−1012.
(15) Cai, S.; Wang, L. Mutual solubilities of selected solvents and 1-(2-hydroxyethyl)-3-methylimidazolium tetrafluoroborate. *Phys. Chem. Liq.* **2011**, *49*, 97−107.
(16) Renon, H.; Prausnitz, J. M. Local compositions in thermodynamic excess functions of liquid mixtures. *AIChE J.* **1968**, *114*, 135−144.
(17) Simulation Software: *ASPEN PLUS of ASPENTECH, Aspen Physical Properties System 2004.1 Physical Property Methods and Models*; Aspen Technology Inc: Cambridge, MA, 2004; pp 2141−2201.
(18) Ko, M.; Im, J.; Sung, J. Y.; Kim, H. Liquid−liquid equilibria for the binary systems of sulfolane with alkanes. *J. Chem. Eng. Data* **2007**, *52*, 1464−1467.
(19) Riddick, J. A.; Bunger, W. B., Sakano, T. K. *Organic Solvents: Physical Properties and Methods of Purification*, 4th ed.; Techniques of Chemistry, Vol. *II*; Wiley-Interscience: New York, 1986.
(20) TRC. *Thermodynamic Tables Non-Hydrocarbons & Hydrocarbons*; Thermodynamic Research Center, Texas A&M University System: College Station, TX, 1965.
(21) Ortega, J.; Plácido, J. Excess enthalpy of some alpha, omega-dichloroalkane (C2−C6) + normal alkane (C5−C17) mixtures. *Int. Data Ser., Sel. Data Mixtures, Ser. A* **1993**, *21*, 1−37.
(22) García Gimenez, P.; Martinez-Lopez, J. F.; Artal, M.; Velasco, I.; Otín, S. Excess enthalpies and isothermal (vapor+liquid) equilibria of (1-methyl-2-pyrrolidone+1-chloroalkane or + α,ω-dichloroalkane) mixtures. *J. Chem. Thermodyn.* **2008**, *40*, 973−979.
(23) García Gimenez, P.; Martinez-Lopez, J. F.; Blanco, S. T.; Velasco, I.; Otín, S. Density and isothermal compressibilities at pressure up to 20 MPa of the Systems *N*,*N*-dimethylformamide or *N*,*N*-dimethylacetamide + α,ω-dichloralkane. *J. Chem. Eng. Data* **2007**, *52*, 2368−2374.
(24) Artal, M.; Muñoz-Embid, J.; Velasco, I.; Otin, S. Analysis of {[α,ω-dichloalkane or α,ω-dibromoalkane] + benzene and α,ω-dichloroalkane + tetrachloromethane} mixtures in terms of group contributions. *Phys. Chem. Liq.* **2000**, *38*, 537−551.
(25) Bandrés, I.; Giner, B.; Artigas, H.; Royo, F. M.; Lafuente, C. Thermophysic comparative study of two isomeric pyridinium-based ionic Liquids. *J. Phys. Chem. B* **2008**, *112*, 3077−3084.
(26) Ortega, J.; Matos, J. S.; Paz, M. I.; Fernández, J. Excess molar volumes of ethyl formate or ethyl acetate+1-chloroalkane at 298.15. *J. Chem. Eng. Data* **1987**, *32*, 464−466.
(27) García-Giménez, P.; Gil-Hernández, V.; Velasco, I.; Emid, J. M.; Otín, S. Temperature and pressure dependence of the volumetric properties of binary liquid mixtures containing dihaloalkanes. *Int. J. Thermophys.* **2005**, *26*, 665−678.
(28) Ortega, J.; Plácido, J. *Int. Data Ser. Sel. Data Mixtures Ser. A.* **1995**, *26*, 285−319.
(29) Mussari, L.; Postigo, M.; Lafuente, C.; Royo, F. M.; Urieta, J. S. Viscosity measurements for the binary mixtures of 1,2-dichloroethane or 1,2-dibromoethane with isomeric butanols. *J. Chem. Eng. Data* **2000**, *45*, 86−91.
(30) Ernst, S.; Zewski, M. C.; Trkaczyk, M.; Goralski, P. Heat capacities and densities of α,ω-dibromoalkanes as functions of temperature a group additivity analysis. *Fluid Phase Equilib.* **2000**, *174*, 33−39.
(31) Blanco, S.; Muñoz, J.; Velasco, I.; Otín, S. Excess molar enthalpies of binary mixtures containing mono- and polybromoalkanes at 298.15 K. *J. Chem. Eng. Data* **1995**, *40*, 605−606.
(32) Vidal, M.; Ortega, J.; Placido, J. Excess enthalpies of 12 binary liquid mixtures of α,ω-dibromoalkanes (C2, C4, C6) + benzene, toluene, ethylbenzene, or butylbenzene at 298.15 K. *ELDATA: Int. Electron. J. Phys. Chem. Data* **1996**, *2*, 121−130.
(33) Vidal, M.; Ortega, J.; Placido, J. Thermodynamic properties of (an ethyl ester + an *n*-alkane) IX. H^E and V^E for $\{x CH_3(CH_2)_u COOCH_2CH_3 + (1-x)\ CH_3(CH_2)_{2v}+1CH_3\}$ with u = 0 to 5, and v = 1 to 7. *J. Chem. Thermodyn.* **1997**, *29*, 47−74.
(34) Ortega, J.; Espiau, F.; Vreekamp, R.; Tojo, J. Modeling and Experimental Evaluation of Thermodynamic Properties for Binary Mixtures of Dialkylcarbonate and Alkanes Using a Parametric Model. *Ind. Eng. Chem. Res.* **2007**, *46*, 7353−7366.
(35) Espiau, F.; Ortega, J.; Penco, E.; Wisniak, J. Advances in the correlation of thermodynamic properties of binary systems applied to methanol mixtures with butyl esters. *Ind. Eng. Chem. Res.* **2010**, *49*, 9548−9558.
(36) Gadhi, J.; Wlodarczak, G.; Legrand, J.; Demaison, J. The dipole moments of methyl bromide and methyl iodide. *Chem. Phys. Lett.* **1989**, *156*, 401−404.
(37) Schröder, U.; Wadhawan, J. D.; Compton, R. G.; Marken, F.; Suarez, P. A. Z.; Consorti, C. S.; de Souza, R. F.; Dupont, J. Water-induced accelerated ion diffusion: Voltammetric studies in 1-methyl-3-[2,6-(*S*)-dimethylocten-2-yl] imidazolium tetrafluoroborate, 1-butyl-3-methylimidazolium tetrafluoroborate and hexafluorophosphate ionic liquids. *New J. Chem.* **2000**, *24*, 1009−1015.
(38) Canongia-Lopes, J. N. A.; Pádua, A. H. Nanostructural organization in ionic liquids. *J. Phys. Chim. B* **2006**, *110*, 3330−3335.
(39) Hradetzky, G.; Bittrich, H.-J. Liquid−liquid equilibrium data for methanol +hexane mixture. *Int. Data Ser.: Sel. Data Mixtures* **1986**, *24*, 216.
(40) Blanco, A. M.; Ortega, J. Experimental study of miscibility, density and isobaric vapor−liquid equilibrium values for mixtures of methanol in hydrocarbons (C5, C6). *Fluid Phase Equilib.* **1996**, *122*, 207−222.